



# Aerosol jet printed capacitive strain gauge for soft structural materials

November 2020

*Changing the World's Energy Future*

Kiyo T Fujimoto, Jennifer K Watkins, Doug Litteken, Timothy Phero, Kevin Tsai, Takoda Bingham, Kshama Lakshmi Ranganatha, Benjamin C. Johnson, Zhangxian Deng, David Estrada, Brian Jaques



#### **DISCLAIMER**

This information was prepared as an account of work sponsored by an agency of the U.S. Government. Neither the U.S. Government nor any agency thereof, nor any of their employees, makes any warranty, expressed or implied, or assumes any legal liability or responsibility for the accuracy, completeness, or usefulness, of any information, apparatus, product, or process disclosed, or represents that its use would not infringe privately owned rights. References herein to any specific commercial product, process, or service by trade name, trade mark, manufacturer, or otherwise, does not necessarily constitute or imply its endorsement, recommendation, or favoring by the U.S. Government or any agency thereof. The views and opinions of authors expressed herein do not necessarily state or reflect those of the U.S. Government or any agency thereof.

# **Aerosol jet printed capacitive strain gauge for soft structural materials**

**Kiyo T Fujimoto, Jennifer K Watkins, Doug Litteken, Timothy Phero, Kevin Tsai,  
Takoda Bingham, Kshama Lakshmi Ranganatha, Benjamin C. Johnson,  
Zhangxian Deng, David Estrada, Brian Jaques**

**November 2020**

**Idaho National Laboratory  
Idaho Falls, Idaho 83415**

**<http://www.inl.gov>**

**Prepared for the  
U.S. Department of Energy  
Under DOE Idaho Operations Office  
Contract DE-AC07-05ID14517, DE-AC07-05ID14517**

# Aerosol Jet Printed Capacitive Strain Gauge for Soft Structural Materials

**Kiyo T. Fujimoto**<sup>1,2,3</sup>: Kiyo.Fujimoto@inl.gov

**Jennifer K. Watkins**<sup>1,2,4</sup>: Jennifer.Watkins@inl.gov

**Timothy Phero**<sup>1,2</sup>: Timothyphero@u.boisestate.edu,

**Doug Litteken**<sup>5</sup>: Douglas.Litteken@nasa.gov,

**Kevin Tsai**<sup>3</sup>: Kevin.Tsai@inl.gov

**Brian Jaques**<sup>1,2</sup>: Brianjaques@boisestate.edu

**Takoda Bingham**<sup>6</sup>: Takodabingham@u.boisestate.edu

**Kshama Lakshmi Ranganatha**<sup>7</sup>: Kshamalakshmiran@u.boisestate.edu

**Zhangxian Deng**<sup>6</sup>: [Zhangxiandeng@boisestate.edu](mailto:Zhangxiandeng@boisestate.edu)

**Benjamin Johnson**<sup>7</sup>: Bcjohnson@boisestate.edu

**David Estrada**<sup>1,2\*</sup>: Daveestrada@boisestate.edu

<sup>1</sup>Center for Advanced Energy Studies, Boise State University, Idaho Falls, ID USA

<sup>2</sup>Micron School of Materials Science and Engineering, Boise State University, Boise, ID USA

<sup>3</sup>Measurement Sciences Department, Idaho National Laboratory, Idaho Falls, ID 83402 USA

<sup>4</sup>Department of Advanced Fuel Manufacturing and Development, Idaho National Laboratory,  
Idaho Falls, ID USA

<sup>5</sup>NASA Johnson Space Center, Houston, TX USA

<sup>6</sup>Department of Mechanical Engineering, Boise State University, Boise, ID USA

<sup>7</sup>Department of Electrical and Computer Engineering, Boise State University, Boise, ID USA

25

26

27

28

29 **Aerosol Jet Printed Capacitive Strain Gauge for**

30 **Soft Structural Materials**

31

32 Kiyoto T. Fujimoto<sup>1,2,3</sup>, Jennifer K. Watkins<sup>1,2,4</sup>, Timothy Phero<sup>1,2</sup>, Kevin Tsai<sup>3</sup>, Doug Litteken<sup>5</sup>,

33 Brian Jaques<sup>1,2</sup>, David Estrada<sup>1,2\*</sup>

34 \*To whom correspondence be addressed: daveestrada@boisestate.edu

35 <sup>1</sup>Center for Advanced Energy Studies, Boise State University, Idaho Falls, ID USA

36 <sup>2</sup>Micron School of Materials Science and Engineering, Boise State University, Boise, ID USA

37 <sup>3</sup>Department of Measurement Sciences, Idaho National Laboratory, Idaho Falls, ID 83402 USA

38 <sup>4</sup>Department of Advanced Fuel Manufacturing and Development, Idaho National Laboratory,

39 Idaho Falls, ID USA

40 <sup>5</sup>NASA Johnson Space Center, Houston, TX USA

41 **Abstract**

42 Soft structural textiles, or softgoods, are used within the space industry for inflatable habitats,

43 parachutes and decelerator systems. Evaluating the safety and structural integrity of these

44 systems occurs through structural health monitoring systems (SHM), which integrate non-

45 invasive/non-destructive testing methods to detect, diagnose, and locate damage. Strain/load

46 monitoring of these systems is limited while utilizing traditional strain gauges as these gauges

47 are typically stiff, operate at low temperatures, and fail when subjected to high strain that is a

48 result of high loading classifying them as unsuitable for SHM of soft structural textiles. For this

work, a capacitance based strain gauge (CSG) was fabricated via aerosol jet printing (AJP) using silver nanoparticle ink on a flexible polymer substrate. Printed strain gauges were then compared to a commercially available high elongation resistance based strain gauge (HE-RSG) for their ability to monitor strained Kevlar straps having a 26.7 kN (6 klbf) load. Dynamic, static and cyclic loads were used to characterize both types of strain monitoring devices. Printed CSGs demonstrated superior performance for high elongation strain measurements when compared to commonly used HE-RSGs, and were observed to operate with a gauge factor of 5.2 when the electrode arrangement was perpendicular to the direction of strain.

## **Keywords**

Aerosol jet printing, strain gauge, high strength textile, structural health monitoring, high elongation strain testing, flexible sensor

## **1. Introduction**

Soft structural textiles, also known as softgoods, that are lightweight while also exhibiting high strength are of particular interest to the space industry for inflatable habitats, parachutes and decelerator systems. The advantages of these technical textiles over traditional structural materials such as metal alloys and rigid composites are found in the significant mass and volume savings that they provide<sup>1</sup>. Benefits aside, complexities emerge from the need to incorporate non-destructive/non-invasive testing methods for structural health monitoring (SHM), which requires monitoring systems capable of measuring very high rates of strain<sup>2</sup>. SHM systems for inflatable habitats, parachutes and decelerating systems are used to ensure the safety of crewmembers, aim to establish an emergency notification system, and enable smart entry, descent, and landing (EDL) operations. Ideally, SHM systems for these applications would provide continuous monitoring of strain/load to detect, diagnose and locate damage in real time for continuous monitoring and also after incident<sup>3</sup>.

73

74 Detecting mechanical deformations is achieved with a variety of sensing mechanisms such as  
75 capacitance, resistance or piezoelectric properties. However, the most widely used strain sensing  
76 devices, are resistance-based strain gauges (RSG)<sup>4</sup>. Traditionally, strain gauges are intended for  
77 use with metals, they employ relatively stiff substrates, operate most effectively at room  
78 temperature before corrections must be incorporated, experience strains under 5%, **display**  
79 **hysteresis in long-term testing, and undergo mechanical failure at higher strains<sup>2-5</sup>**. When  
80 considering soft structural materials strain gauges must be capable of withstanding high rates of  
81 strain **(5-50%) associated with materials being under high load**, but the inherent stiffness of  
82 traditional strain gauges results in device failure, and classifies them as unsuitable for the  
83 inspection of soft structural materials<sup>3,5</sup>. Additional limitations of the more popular RSGs are  
84 found in the dependence of resistivity upon operating temperature and applied strain<sup>4,6,7</sup>.  
85 Dependencies such as this result in a non-linear strain response and device hysteresis caused by  
86 variable sensitivity as the gauge factor does not remain constant during testing<sup>6-8</sup>. **Finally, the**  
87 **fabrication of traditional strain sensors involves complex preparation processes resulting in high**  
88 **fabrication cost and material waste, which can limit their application and development.** Hence,  
89 developing strain sensing methods for soft structural materials requires the ability to fabricate  
90 devices having high flexibility and a robustness that enables them to withstand harsh  
91 environments to include high strain and high temperatures.

92

93 Capacitance based strain gauges(CSGs) provide a robust sensing mechanism capable of  
94 addressing the performance issues associated with resistivity hysteresis of RSGs. CSGs are  
95 largely dependent on geometry changes between the electrodes and the dielectric layer which  
96 typically do not suffer permanent plastic deformation during cyclical testing<sup>2,9</sup>. These devices, in

general, include parallel-plate capacitors or an interdigitated electrode design<sup>4,5,10,11</sup>. CSGs can be used for many of the same applications as RSGs, and typically display higher gauge factors of 15-30, while also having reduced sensitivity to noise and temperature<sup>2</sup>. Currently, commercial CSGs are available, and typically consist of a parallel plate design restricting strain measurements to those that are perpendicular to the gauge direction, are limited in the geometries they can monitor, or require bulky electromechanical devices for mechanical attachment<sup>2,12</sup>. These issues can be overcome by using CSGs having an interdigitated electrode design<sup>13,24</sup>. Interdigitated electrodes preserve the advantages associated with CSGs vs RSGs in harsh environments, while also providing a vehicle by which CSGs can integrate directly onto structural components. Previous testing has been conducted on Kevlar webbing with flexible strain gauges and it was concluded that CSGs performed better than RSGs in dynamic and long term loading conditions similar to those that were investigated within this work<sup>3</sup>. Finally, using capacitance as the sensing mechanism makes the sensor more suitable for applications where wireless strain sensor measurements are required<sup>10,14</sup>. This would be tremendously advantageous for SHM during smart EDL operations.

Introducing the flexibility needed for SHM of soft structural materials can be achieved by making use of recent advances in additive manufacturing for printed and flexible electronics. Additive manufacturing techniques such as aerosol jet printing (AJP) are relatively simple and low-cost manufacturing processes that can be used to fabricate flexible CSGs where typical substrates employed for flexible applications include polyimide, polyethylene terephthalate and polydimethylsiloxane<sup>2,15-18</sup>. Printed electronics involve the use of a functional material in the form of a nanoparticle suspension, or ink, that is then deposited onto a flexible polymer backing. After deposition, the solvent and dispersing/capping agents are removed to produce a functional



device, which is then attached to either the users clothing or skin. This cross-cutting technology demonstrates significant potential for SHM of soft structural materials as the functionality of these devices are dependent upon their high flexibility, long durability, fast response, fast recovery time and high sensitivity to strain.

The AJP technology is a non-contact deposition based on the atomization of inks to form a fine mist or aerosol that is deposited on a substrate. The aerosol jet process eliminates many of the limitations associated with conventional fabrication methods by introducing the ability to print with a wide range of materials such as metal nanoparticles, carbon nanomaterial, functional ceramics, semiconductors, biological molecules and other functional materials as inks can range from 1-2500 cP<sup>15,19–23</sup>. Additionally, device designs are no longer material or geometry limited as AJP introduces the ability to print on a variety of substrates/surfaces, and provides a wide range of feature sizes that span 10  $\mu\text{m}$  to 5 mm<sup>24–27</sup>. With the ability to achieve higher print resolutions, AJP has the potential to enhance device sensitivity by maximizing the design space of structural health monitoring systems, and provides a low-cost option for sensor fabrication<sup>28,29,30</sup>.

In this work we report, **for the first time**, on the response of aerosol jet printed **flexible** CSGs having an interdigitated electrode design (adapted from Hu *et al.*) **targeted for use on soft structural materials**<sup>31</sup>. The strain response of these printed gauges was then compared to that of commercially available high elongation resistance-based foil strain gauges (HE-RSG). This comparison was used to evaluate the benefits of utilizing the advanced manufacturing technique of AJP to fabricate a robust and flexible strain gauge, while also serving to validate the advantages of a capacitive sensor for measuring the strain of soft structural materials. Flexible

CSGs were fabricated via AJP using silver nanoparticle ink and a flexible polymer substrate to monitor military grade Kevlar webbing under high load as this material is typically used in EDL operations and inflatable habitat structures. However, the focus of this work was towards inflatable habitats. Dynamic, static, and cyclic loads were used to characterize both types of strain monitoring devices. Printed CSGs demonstrated superior performance for high elongation strain measurements of Kevlar webbing when under high load when compared to commonly used HE-RSGs and were observed to operate with a gauge factor of 5.2 when an electrode arrangement perpendicular to the direction of strain was used.

## 2. Results and Discussion

### 2.1. Interdigitated Electrode Geometry

Military grade Kevlar webbing is used for the construction of inflatable habitats and parachutes, and the ability to measure the strain experienced by these structures is a challenge for NASA<sup>3</sup>. To produce a capacitive strain gauge, an interdigitated structure was employed, which operates in a similar manner to having multiple parallel plate capacitors in series. A schematic representation of the device layout can be found in Figure 1a, and an optical image of the actual printed sensor in Figure 1b. Capacitance was a result of an interdigitated structure spanning 3.6 cm and 1.6 cm with 50 digit pairs or 100 total electrodes. These specific design parameters were chosen in order to maximize both the theoretical capacitance and the sensing area. Additionally, size limitations were associated with the capabilities of the aerosol jet printing technology, and the 2.54 cm wide Kevlar webbing. Silver epoxy was used to attach copper wire leads to the device, and poly methyl methacrylate (PMMA), having a dielectric constant of 5.70, was used both as a protective layer and as the dielectric between the electrodes to enhance the device capacitance over what could be achieved if air served the same function<sup>20</sup>. Finally, Kapton (FPC

5 mil, 125  $\mu\text{m}$ ) was selected as the flexible substrate as it is capable of withstanding elongation that is significantly higher than the maximum elongation of the Kevlar straps when subjected to maximum loading capacity<sup>32</sup>.

In Figure 2, representative higher magnification images of the digits a.) center and b.) ends along with their respective height profiles shown in Figure 2c. As depicted, the electrode morphology varies due to the formation of a bulb-like structure at the electrode ends where variation is seen in both height and width. Rahman *et al.* reported the formation of a similar feature at the ends of their printed electrodes while also stating that this change in morphology could be controlled by increasing the printer's shutter speed while using Clariant Prelect TPS 50G2 with the ultrasonic atomizer<sup>33</sup>.

For this study, devices were printed using the pneumatic atomizer for a silver nanoparticle based ink, PvNanoCell Sicrys™ 160PM-116, known for having excellent adhesive properties with a variety of substrates, and near bulk resistivity ( $10^{-6} \Omega\cdot\text{cm}$ ). During the printing process the shutter speed is ultimately controlled by the “rapid” process speed, which controls the speed at which the printer platen moves between depositions. For the fabrication of the CSGs the maximum rapid speed was used, but the formation of the bulb resulted despite modifications to other print parameters such as atomizer, exhaust, and sheath flow rates. This demonstrates that the quality of the print and ultimately the device is dependent upon the ink and atomization process being used.

## 2.2. CSG Structure

To further characterize the structure of the printed CSG, cross-sectional SEM was performed to investigate both the quality of the printed CSG and that of the dielectric layer (Figure 2d). Preparing the sample for imaging required the device to be mounted in Quickstick 135 mounting wax prior to slicing with a microtome, and finally the cross-section was carbon coated to minimize surface charging while imaging. A top-down view of the overspray is provided in Figure 2a, and a cross-section view is presented in Figure 2e with the overspray creating a “tail” on either end of the digit. From Figure 2e, the overspray is more pronounced on the left side of the digit, which indicates that N<sub>2</sub> flow was not symmetrical through the nozzle and/or the virtual impactor. The PMMA layer was uniform having a thickness of  $10.2 \pm 0.1 \mu\text{m}$  demonstrating that the drop cast method is an effective way of encapsulating the digits, which is crucial for maximizing the measured capacitance of CSG devices. The maximum thickness of the digit was  $2.7 \pm 0.1 \mu\text{m}$ , which is in good agreement with results obtained from stylus profilometry ( $2.2 \pm 0.5 \mu\text{m}$ ). The cross-section profile shows the porous nature of the printed structure, and with image analysis software the porosity was determined to be  $16.1 \pm 0.4\%$  of the total electrode volume. Gaps/voids providing a porous structure are an inherent feature found within AM devices that is highly dependent upon the ink being printed<sup>26</sup>.

### *Electrical Characterization*

The theoretical initial capacitance,  $C_0$ , and theoretical strained capacitance,  $C_N$ , were derived from previous work by Hu *et al.* and Kim *et al.*, and are expressed by<sup>4,31</sup>

$$(1)$$

$$(2)$$

$$(3)$$

where  $p$  is dielectric constant of PMMA,  $t$  is the thickness of the printed silver digit,  $l$  is the length of the digit,  $a$  is the total width of the interdigitated electrodes,  $w$  is the width of the digit,  $n$  is the number of digit pairs,  $d$  is the spacing between the digits of the electrodes,  $\epsilon_0$  is the permittivity of free space. The expected change in capacitance resulting from a strain incident perpendicular and parallel to electrode orientation is depicted in eq(2) and eq(3), respectively. Briefly, when the device experiences strain perpendicular to electrode orientation the spacing between electrodes is expected to increase by a factor of  $d_0(1+\nu)$ . However, due to poisson contraction, it is expected that  $a$ ,  $w$  and  $l$  will change by a factor of  $(1-\nu)$  from their original values, where  $\nu$  is the poisson ratio of the encapsulating polymer. For the printed CSGs, the encapsulating material is PMMA with a poisson ratio of 0.37<sup>34</sup>. With this phenomenon it is expected that as the PMMA is elongated in one direction it compresses in the two directions perpendicular to the direction of strain<sup>4</sup>. A schematic detailing the variables used in eq(1) and eq(2) is provided in Figure 3a, and the associated dimensions are found within Figure 3b. From the device dimensions, the initial capacitance of the printed CSGs is expected to range from 4.56-6.70 pF. However, the actual capacitance was measured to range between 42 pF and 15 nF, and the initial capacitance values for each device can be found in Table 1. The significant deviation from theoretical capacitance is attributed to the unique geometry of the digit introduced by the printing process, which is evident in Figure 2(a-e) where the electrode structure with trailing ends associated with overspray is observed in addition to a porous structure.

Overspray is caused by the smallest droplets within the aerosol, and can be minimized to some extent by varying the sheath, exhaust, or atomizer flow rates<sup>35,36</sup>. However, overspray, like void

formation, is an inherent feature of aerosol jet printed devices and was found to contribute between 5-25  $\mu\text{m}$  of additional width to the digits. Additionally, an internal capacitance may exist within the digits themselves which is associated with the structure voids themselves with air serving as the dielectric. While AJP provides significant versatility from its compatibility with a broad range of materials, consistency and reproducibility are challenges that need to be overcome. For experienced users, optimizing print parameters to mitigate these challenges can require extreme measures which include, but are not limited to, frequent replacement of ink and extensive time spent towards empirical optimization for this sensitive process<sup>21,23,35,37,38</sup>.

#### *Strain Measurements*

Capacitance and resistance measurements for printed CSGs and commercial RSGs, respectively, were collected for each sample prior to any **load**/strain being imparted to the Kevlar strap, and compared to measurements obtained before the samples were mounted into the test system to verify that no damage to the gauge had occurred during transport and setup. **For each device that was tested the initial capacitance and resistance measurements can be found in Table 1.** Final measurements were recorded for each sample at the conclusion of testing after the strain was released and the strap allowed to relax. However, due to the natural stretch of the Kevlar material the straps did not return to their original dimensions, and were permanently elongated after tensile loading.

Printed CSG's exhibited initial capacitance measurements that ranged from  $\sim 45$  pF to  $\sim 15$  nF **at 10 kHz with a 5 V bias.** As the observed range is significant between the printed strain gauges, representative devices from both the pF and nF regime were originally included with both perpendicular and parallel arrangement of electrodes with respect to the direction of strain.

However, the device detached during dynamic testing with the representative nF device with electrodes parallel to the direction of strain.

As this work was a result of a collaboration with NASA Johnson Space Center, testing was performed in a manner that was in agreement with previously performed testing procedures<sup>3</sup>. The response of both capacitive and resistive devices was investigated while under dynamic, static, and cyclic loading. Mechanical testing was performed by subjecting the Kevlar webbing to targeted loading conditions rather than strain. This was the method for testing due to the fact that variations in the Kevlar webbing, attributed to the weaving process of these textiles, causes samples subjected to the same loading conditions to exhibit a different strain response between samples<sup>32</sup>. As the webbing is rated according to a maximum loading capacity of 26.7 kN, a peak load of 18.7 kN was selected for dynamic and static testing as it is 70% of the maximum capacity of the Kevlar webbing. Furthermore, cyclic testing was performed at targeting loads of 5.3 kN (1.2 klbf) and 10.7 kN (2.4 klbf) or 20% and 40% of maximum loading capacity of the Kevlar webbing, respectively. The targeted loads for dynamic and static testing resulted in a strain response of > 5%, which still classifies the strain at which these samples were subjected to as relatively high. For reference, a summary of experiments can be found in Table 1. Dynamic testing was performed for printed CSGs with electrodes configured perpendicular and parallel to the direction of strain and for HE-RSGs having electrodes arranged parallel to the direction of strain up to a maximum load of 18.7 kN (4.2 klbf), which is 70% of the maximum load capacity of the Kevlar webbing used for testing. Additionally, loading conditions were achieved with a ramp rate of 45 N/sec or (10 lbf/sec). Throughout dynamic testing measurements were collected at 4.4 kN (1.0 klbf), 8.9 kN (2.0 klbf), 13.3 kN (3.0 klbf), 17.8 kN(4.0 klbf) and 18.7 kN (4.2 klbf). For CSGs having electrodes arranged perpendicular to the direction of strain an inverse

relationship was observed as depicted in Figure 4a, where the MRCC (maximum relative change in capacitance) was ~20% for devices having a starting capacitance in the nF regime, and ~3% for a pF starting capacitance. This negative change in capacitance for electrodes positioned perpendicular to the direction of strain is due to the increasing elongation of the strap, which increases the distance between the electrodes resulting in a decrease to the capacitance. The indirect relationship between strain and capacitance was confirmed through 3D finite element modeling. However, the magnitude of relative capacitance change is significantly different, and that is attributed to the device features introduced from the printing process. The results from those efforts can be found in the supporting information. During testing, images were captured at each change, targeted load, and/or time point. Utilizing Digimizer software, and images obtained while testing when electrodes were perpendicular to the direction of strain, the change in distance between the top of the first electrode to the bottom of the last electrode from an applied load of zero to 18.7 kN (4.20 klbF) was determined to be 815  $\mu\text{m}$ . So, as the Kevlar webbing was under high load, the sensor experienced a strain of 0.037 while the webbing experienced an average strain of  $0.060 \pm 0.001$ . With that, a gauge factor of 5.2 obtained for the perpendicular orientation with devices having a starting capacitance within the nF range. In contrast, a direct relationship between load and capacitance was observed for devices with electrodes arranged parallel to the direction of strain. As the strap is elongated, and the polyimide substrate is stretched, the spacing between the electrodes is decreased resulting in larger capacitance values. From Figure 4b the MRCC differed by a factor of 2.3 where the MRCC for Device D was 1.6%, and for Device E was 3.7%. Dynamic testing finished immediately after a maximum load of 18.7 kN (4.2 klbF) had been reached, and static testing began. To demonstrate the printed CSGs ability to maintain a signal while under a constant load, the devices were held for a total of 65 minutes with measurements collected in 5 minute intervals (Figure 4c). As



shown in Figure 4(c,d), while all devices were able to maintain a signal for the duration of testing, the arrangement with electrodes perpendicular to the direction of strain produced a signal having less hysteresis over the observed timeframe. Finally, cyclic testing was conducted for devices having electrodes arranged perpendicular to the direction of strain by cycling between 5.3 kN (1.2 klbf) and 10.7 kN (4.2 klbf) for a total of ten cycles (Figure 4e).

For practical application of the printed CSG's it will be necessary to quickly and efficiently obtain the capacitance read out for analysis while minimizing the effects of interference. The ability to accommodate a large capacitance range from printed strain gauges while having a fast and efficient response can be achieved through the use of a digital read out that uses frequency rather than voltage (Please see supporting info).

Utilizing the same attachment strategy and testing conditions, the resistance behavior of commercially available HE-RSGs having a similar Kapton backing as the CSGs was investigated to compare and evaluate their suitability for SHM of soft structural materials. For HE-RSGs, per manufacturer instruction, the electrodes were positioned parallel to the direction of strain. The mechanism for RSG response to strain is explained with the following relationship

where  $R$  is resistance,  $\rho$  is a material's resistivity,  $L$  is total length foil, and  $A$  is the cross-sectional area of the foil. For strain testing of these Kevlar straps, device elongation occurs with strain, and it is expected that the resistance would increase with increasing load. The response of HE-RSGs during dynamic testing is shown in Figure 5a, where a direct relationship between resistance and load was observed up to 4.4 kN (1 klbf). While this direct relationship is expected, after the load of 4.4 kN is reached the resistance behavior transitions to an indirect relationship

with the applied load at 8.9,13.3,17.8 and 18.7 kN (2, 3, 4, and 4.2 klbf respectively). This behavior indicates that testing conditions may have caused the gauge to exceed its elongation limit, and demonstrates well-known limitations of foil based gauges for high elongation applications<sup>39,40</sup>. For high elongation applications where the plastic elongation conditions are met, the linearity of the strain device can vary as the gauge factor is known to modify using the guideline of  $2+\epsilon$ , where  $\epsilon$  is the strain such that the gauge factor at a strain level of 10% is expected to be around 2.1 in tension<sup>39,33</sup>. Immediately after a maximum load of 18.7 kN (4.2 klbf) was achieved with dynamic testing, static testing began for period of 65 minutes (Figure 5b). Another limitation is revealed during dynamic testing as signal hysteresis is shown to progress over the observed timeframe for all HE-RSG devices, which demonstrates an inability to reliably monitor strain for extended periods of time while under a constant load. Finally, HE-RSGs were subjected to cyclic testing (Figure 5c). Cyclic testing provided further support of the aforementioned limitations of HE-RSGs as similar resistance behavior was observed after the initial target load is achieved, and signal degradation was apparent for each cycle after equilibrium had been achieved. The first cycle reveals that an equilibrium must be established prior to conducting strain measurements as the resistance decreases with the transition from 5.3 kN (1.2 klbf) to 10.7 kN (2.4 klbf). However, the following cycles produce the expected resistance response where an increase in resistance is observed as the applied load increases, and a decrease in resistance is observed as the applied also decreases. Notably, signal hysteresis associated with the HE-RSGs is observed for all three testing conditions and provides evidence that printed CSGs exhibit superior performance with high elongation testing conditions resulting in these devices being considered better suited for SHM for soft structural materials than HE-RSGs.

Finally, variation in initial capacitance values, device response for the first couple of strains, etc., can be compensated for with calibration for the intended application of structural health monitoring of soft structural materials for inflatable habitats. For a crewed, inflatable space habitat, a series of strain sensors would be used in a network for structural health monitoring of the habitat. The sensors would be calibrated on the ground before launch when a precise amount of strain could be applied to the straps. Once the calibration is completed, the strain sensors would be powered off until needed again in space. After launch, deployment, and pressurization, an initial reading would be taken to get a starting strain for the strap material. This strain level would be compared to the levels recorded during the ground calibration testing to ensure no strain changes occurred during the launch phase. While the habitat will stay pressurized during its lifetime, the strain in the straps and in the gage will change over time. This change will be tracked at regular intervals throughout the length of the mission to provide an understanding of the structural health of the habitat.

Initial change during the first couple of strains can be compensated with similar calibration exercises on the ground before launch. The habitat will be testing in the space environment before it's launched and strain changes will be measured. Those strain values are expected to be representative of what would be seen during the initial change in strain once the gages and the habitat are in space. By conducting a series of ground tests, we can fully understand and predict the behavior of the habitat and the strain measurement system and use that prediction to compensate the readings in space.

### **3. Conclusions**

In summary, a capacitive based strain gauge was fabricated via aerosol jet printing where silver

served as the capacitive material and PMMA the dielectric. Printed CSGs exhibited starting capacitance values ranging from 42 pF to 15 nF. A flexible substrate, Kapton, was employed to provide the required flexibility for these devices to withstand high load/strain, and All-purpose Barge Cement served as the adhesive between the Kapton and the Kevlar strap. Dynamic and static testing was performed for arrangements where the electrodes were oriented either perpendicular or parallel to the direction of strain, and the perpendicular arrangement was used for cyclic testing. Furthermore, HE-RSGs were tested utilizing the same attachment strategy, under the same conditions, to compare their response to printed CSGs, and to evaluate their suitability for SHM of soft structural materials. Devices having a starting capacitance in the nF range demonstrated the highest sensitivity, and a gauge factor of 5.2 was obtained for those devices having their electrodes arranged perpendicular to the direction of strain. Finally, printed CSGs were determined to be the better candidates for high elongation application as they performed better in static situations, dynamic and cyclic events when compared to commercially available HE-RSGs.

## **4. Methods**

### **4.1. Device Fabrication.**

The layout of the interdigitated CSG device is shown in Figure 1a. Device fabrication began by depositing Sicrys™ 160PM-116 (PV Nanocell) onto a 125 µm thick DuPont™ Kapton (FPC). Printing was achieved with the pneumatic atomizer (PA) of an Optomec Aerosol Jet 200 equipped with a 200 µm nozzle. While printing, the ink was held at 23°C to stabilize the ink, and the printed films were heated at 300 °C for 30 min. to remove any residual solvent. The tool platen temperature, nozzle diameter, and pneumatic atomizer, pneumatic exhaust and sheath gas flows were optimized to ensure the line widths and material deposition of functional materials

were adequate to obtain conductive traces. Silver epoxy (Epotek, H20E) was used to adhere 30-gauge copper wire to the printed contact pads, and a layer of 950 PMMA A11 (Kayaku Advanced Materials, Inc.) was drop-coated onto the surface of the device to serve as the dielectric. Both the printed CSG and commercially acquired RSG (HBM, Inc., 1-LD20-6/350) devices were attached to Kevlar straps having a maximum loading capacity of approximately 27 kN (6 klbf) with All-Purpose Barge Cement.

#### 4.2. Characterization.

Device imaging and dimensions were obtained by digital microscopy (Keyence VHX-5000), scanning electron microscopy (FEI Teneo Field Emission Scanning Electron Microscopy) and laser microscopy (Keyence VK-Z260K 3D Laser Scanning Confocal Microscope). Additional height profiles were obtained with a Bruker Dektak XT-A Stylus Profilometer fitted with a 2  $\mu\text{m}$  stylus. A Leica EM UC6 microtome equipped with glass blades was used to produce CSG cross-sections. Furthermore, cross-sectioning required devices to first be encapsulated in Quickstick 135 mounting wax (Scanning Microscopy Services) prior to slicing. CSG cross-sections were carbon-coated to prevent charging of the specimen.

#### 4.3. Device Attachment.

Strain gauges were attached to Kevlar webbing (1991-25.4 mm, Type VI, Class 9) nominally rated at 26.7 kN (6 klbf), and manufactured to Mil-T 87130 manufacturing specifications. Attaching the gauges to the Kevlar webbing was accomplished with a contact cement known as APBC (All-Purpose Barge Cement; Barge Cements, Inc.). This cement is a polychloroprene based adhesive that is well known for its high strength and flexibility and is typically used in the leather, shoe and prosthetic industries. While the tensile modulus for APBC is not reported or

available, polychloroprene is reported to have a tensile modulus of 21 MPa<sup>41</sup>. This is well below the tensile modulus for kapton and kevlar, which indicates that it is well-suited for the intended application. For testing purposes, multiple adhesives were considered including Double/Bubble epoxy, Pliobond 25, DAP Cove Base Zocalo construction adhesive, and GE silicone II caulk. However, APBC was the only adhesive capable of maintaining the integrity of the bond while under high strain such as that produced while testing Kevlar straps. Adhering the printed CSGs and RSGs to the Kevlar strap began by applying a thin layer of APBC to both the testing strap and the backside of the printed CSG or RSG. The two items were immediately bonded together with the adhesive sandwiched between the CSG or RSG backing and the strap. The bond was allowed to cure for 24 hours.

#### 4.4. Testing.

After the bond was fully cured the Kevlar straps were attached to the webbing grips on the MTS test system by wrapping each end of the strap at least three times around the grip to ensure the strap would not come loose during testing. The grips were positioned such that there was approximately 24" between the base of each grip with the strain gauge positioned in the center. Samples tested included gauges mounted with electrodes both perpendicular and parallel to the direction of strain resulting in positive and negative changes in capacitance respectively. The leads to the LCR meter were attached and supported to ensure the leads would not come into contact with each other, would not place undue tension on the copper wire attachments, and would remain relatively stable during testing. CSG devices were attached both perpendicular and parallel to the direction of strain while RSG devices were only tested having electrodes parallel to the direction of strain, and both types of devices were attached to Kevlar straps with All-Purpose Barge Cement. Strain testing was performed with an MTS 810 Material Test

System equipped with a 100 kN load head, ADMET GRW-50T (Part No. 3218-00225) webbing grips, and FlexTest SE Station Manager software. Capacitance measurements were obtained with an Agilent HP 4284A Precision LCR Meter (10 kHz at 5V), and resistance measurements were obtained with a Keithley 2182A/6220 (-1 to 1 mA, Printed CSG and commercial RSG devices were studied under dynamic, cyclic, and static loads while Kevlar straps were subjected to a maximum load of 18.7 kN (4.2 klbf) during static and dynamic loads at a ramp rate of 45 N/sec (10 lbf/sec). During dynamic testing capacitance measurements were obtained every 4.5 kN (1 klbf) up to the maximum load of 18.7 kN (4.2 klbf), and static loads were held for a total of one hour ten minutes with capacitance measurements taken every five minutes. Additionally, printed CSGs and commercial RSGs were characterized under cyclic loading of 5.3 kN (1.2 klbf) and 10.7 kN (2.4 klbf) for ten total cycles with a ramp rate of 89 N/sec (20 lbf/sec) with capacitance measurements taken at 90 second intervals between5. each cycle. Macro images of the CSGs were taken in tandem with capacitance measurements in order to determine the gauge factor for the CSGs. Images were recorded with a Canon EOS 70D digital SLR camera outfitted with a Tamron AF 90mm f/2.8 1:1 macro lens. The camera was held stationary on a tripod and a remote trigger was used to eliminate vibration during image exposure. The ruler imaged next to the CSG during testing was kept in-plane with the device for use in measuring the dimensional change experienced by the CSG at strain. Gauge factor calculations were completed using values for the dimensional changes obtained in conjunction with digital imaging processing software.

#### **Data availability**

The data that supports the findings of this study are available from the authors on reasonable request, see author contributions for specific data sets.

#### **Acknowledgments**

This material is based upon work supported under an Integrated University Program Graduate Fellowship, and was supported in part by Department of Energy In-Pile Instrumentation program under DOE Idaho Operations Office Contract DE-AC07-05ID14517 and by the National Aeronautics Space Administration under award #80NSSC18M0088. The views and opinions of authors expressed herein do not necessarily state or reflect those of the U.S. Government or any agency thereof. D.E. also acknowledges career development support by Institutional Development Awards (IDeA) from the National Institute of General Medical Sciences of the National Institutes of Health under Grants #P20GM103408 and P20GM109095.

#### **Author Contributions**

K.F. designed and printed the test structures, and together with J.W., K.T. characterized the devices. J.W., K.F., D.L. and D.E. conceived of the experimental design and together with B.J., supervised the experiments. K.F., J.W., and T.P. performed the mechanical testing of all strain gauges. All authors contributed to the development of the manuscript.

#### **Competing Interests**

The authors declare no competing interests.



## References

1. Hinkle, J. *et al.* Intelligent Flexible Materials for Space Structures Expandable Habitat Engineering Development Unit. (2010).
2. Li, J., Longtin, J. P., Tankiewicz, S., Gouldstone, A. & Sampath, S. Interdigital capacitive strain gauges fabricated by direct-write thermal spray and ultrafast laser micromachining. *Sensors Actuators, A Phys.* **133**, 1–8 (2007).
3. Litteken, D. Evaluation of Strain Measurement Devices for Inflatable Structures. in (American Institute of Aeronautics and Astronautics (AIAA), 2017).  
doi:10.2514/6.2017-0426
4. Kim, S. R., Kim, J. H. & Park, J. W. Wearable and Transparent Capacitive Strain Sensor with High Sensitivity Based on Patterned Ag Nanowire Networks. *ACS Appl. Mater. Interfaces* **9**, 26407–26416 (2017).
5. Cohen, D. J., Mitra, D., Peterson, K. & Maharbiz, M. M. A highly elastic, capacitive strain gauge based on percolating nanotube networks. *Nano Lett.* **12**, 1821–1825 (2012).
6. Amjadi, M., Pichitpajongkit, A., Lee, S., Ryu, S. & Park, I. Highly stretchable and sensitive strain sensor based on silver nanowire-elastomer nanocomposite. *ACS Nano* **8**, 5154–5163 (2014).
7. Andeen, C., Fontanella, J. & Schuele, D. A capacitive gauge for the accurate measurement of high pressures. *Rev. Sci. Instrum.* **42**, 495–496 (1971).
8. Amjadi, M., Kyung, K. U., Park, I. & Sitti, M. Stretchable, Skin-Mountable, and Wearable Strain Sensors and Their Potential Applications: A Review. *Adv. Funct. Mater.* **26**, 1678–1698 (2016).
9. Lipomi, D. J. *et al.* Skin-like pressure and strain sensors based on transparent

- elastic films of carbon nanotubes. *Nat. Nanotechnol.* **6**, 788–792 (2011).
10. Tsouti, V., Mitrakos, V., Broutas, P. & Chatzandroulis, S. Modeling and Development of a Flexible Carbon Black-Based Capacitive Strain Sensor. *IEEE Sens. J.* **16**, 3059–3067 (2016).
11. Matsuzaki, R. & Todoroki, A. Wireless flexible capacitive sensor based on ultra-flexible epoxy resin for strain measurement of automobile tires. *Sensors Actuators, A Phys.* **140**, 32–42 (2007).
12. Glass, S. W., Fifield, L. S., Sriraman, A. & Bowler, N. Inter-digital capacitive sensor for evaluating cable insulation through jacket. *19th Int. Conf. Environ. Degrad. Mater. Nucl. Power Syst. - Water React. EnvDeg 2019* **020024**, 852–858 (2019).
13. Zeiser, R., Fellner, T. & Wilde, J. Capacitive strain gauges on flexible polymer substrates for wireless, intelligent systems. *J. Sensors Sens. Syst.* **3**, 77–86 (2014).
14. Lynch, J. P. A Summary Review of Wireless Sensors and Sensor Networks for Structural Health Monitoring. *Shock Vib. Dig.* **38**, 91–128 (2006).
15. Cao, C., Andrews, J. B. & Franklin, A. D. Completely Printed, Flexible, Stable, and Hysteresis-Free Carbon Nanotube Thin-Film Transistors via Aerosol Jet Printing. *Adv. Electron. Mater.* **3**, (2017).
16. Cheng, M. Y., Lin, C. L., Lai, Y. T. & Yang, Y. J. A polymer-based capacitive sensing array for normal and shear force measurement. *Sensors (Switzerland)* **10**, 10211–10225 (2010).
17. Wang, F. X. *et al.* Aerosol-jet printing of nanowire networks of zinc octaethylporphyrin and its application in flexible photodetectors. *Chem. Commun.* **49**, 2433–2435 (2013).
18. Obata, K. *et al.* Hybrid 2D patterning using UV laser direct writing and aerosol jet

- p>
printing of UV curable polydimethylsiloxane.
- Appl. Phys. Lett.*
- 111**
- , (2017).
19. Feng, J. Q. & Renn, M. J. Aerosol Jet ® Direct-Write for Microscale Additive Manufacturing .
- J. Micro Nano-Manufacturing*
- 7**
- , 011004 (2019).
20. Wilkinson, N. J., Smith, M. A. A., Kay, R. W. & Harris, R. A. A review of aerosol jet printing—a non-traditional hybrid process for micro-manufacturing.
- Int. J. Adv. Manuf. Technol.*
- (2019). doi:10.1007/s00170-019-03438-2
21. Secor, E. B. Principles of aerosol jet printing.
- Flex. Print. Electron.*
- 3**
- , (2018).
22. Folgar, C. E., Suchicital, C. & Priya, S. Solution-based aerosol deposition process for synthesis of multilayer structures.
- Mater. Lett.*
- 65**
- , 1302–1307 (2011).
23. Mahajan, A., Frisbie, C. D. & Francis, L. F. Optimization of aerosol jet printing for high-resolution, high-aspect ratio silver lines.
- ACS Appl. Mater. Interfaces*
- 5**
- , 4856–4864 (2013).
24. Paulsen, J. A., Renn, M., Christenson, K. & Plourde, R. Printing conformal electronics on 3D structures with aerosol jet technology.
- FIIW 2012 - 2012 Futur. Instrum. Int. Work. Proc.*
- 47–50 (2012). doi:10.1109/FIIW.2012.6378343
25. Hedges, M., Borrás, A. & Services, M. N.
- 3D Aerosol Jet ® Printing-Adding Electronics Functionality to RP/RM*
- .
26. Pandhi, T.
- et al.*
- Electrical Transport and Power Dissipation in Aerosol-Jet-Printed Graphene Interconnects.
- Sci. Rep.*
- 8**
- , (2018).
27. Deiner, L. J. & Reitz, T. L. Inkjet and Aerosol Jet Printing of Electrochemical Devices for Energy Conversion and Storage.
- Advanced Engineering Materials*
- 19**
- , (2017).
28. Madou, M. J. Manufacturing Techniques for Microfabrication and Nanotechnology. in
- Manufacturing Techniques for Microfabrication and Nanotechnology*
- 521 (2011).

29. Morales-Rodriguez, M. E., Joshi, P. C., Humphries, J. R., Fuhr, P. L. & McIntyre, T. J. Fabrication of low cost surface acoustic wave sensors using direct printing by aerosol inkjet. *IEEE Access* **6**, 20907–20915 (2018).
30. Sethumadhavan, V., Saraf, S. & Chaudhari, A. Development of printable electronic materials for low cost flexible sensor fabrication. *Proc. - 2017 IEEE Int. Conf. Electr. Instrum. Commun. Eng. ICEICE 2017* **2017-Decem**, 1–5 (2017).
31. Hu, C. F., Wang, J. Y., Liu, Y. C., Tsai, M. H. & Fang, W. Development of 3D carbon nanotube interdigitated finger electrodes on polymer substrate for flexible capacitive sensor application. *Nanotechnology* **24**, (2013).
32. Selig, M. M. *et al.* Creep burst testing of a woven inflatable module. *2nd AIAA Spacecr. Struct. Conf.* 1–23 (2015). doi:10.2514/6.2015-1625
33. Rahman, M. T., Rahimi, A., Gupta, S. & Panat, R. Microscale additive manufacturing and modeling of interdigitated capacitive touch sensors. *Sensors Actuators, A Phys.* **248**, 94–103 (2016).
34. MatWeb. Overview of materials for Acrylic , Cast MatWeb , Your Source for Materials Information - WWW . MATWEB . COM / MatWeb , Your Source for Materials Information - WWW . MATWEB . COM /. 1–2
35. Chen, G., Gu, Y., Tsang, H., Hines, D. R. & Das, S. The Effect of Droplet Sizes on Overspray in Aerosol-Jet Printing. *Adv. Eng. Mater.* **20**, (2018).
36. Verheecke, W., Van Dyck, M., Vogeler, F., Voet, A. & Valkenaers, H. Optimizing aerosol jet® printing of silver interconnects on polyimide film for embedded electronics applications. *8th Int. DAAAM Balt. Conf. "INDUSTRIAL Eng.* 373–379 (2012).
37. Salary, R. (Ross) *et al.* Computational Fluid Dynamics Modeling and Online

Monitoring of Aerosol Jet Printing Process. *J. Manuf. Sci. Eng.* **139**, 021015 (2016).

38. Gu, Y., Gutierrez, D., Das, S. & Hines, D. R. Ink wells for on-demand deposition rate measurement in aerosol-jet based 3D printing. *J. Micromechanics Microengineering* **27**, (2017).

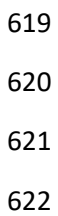
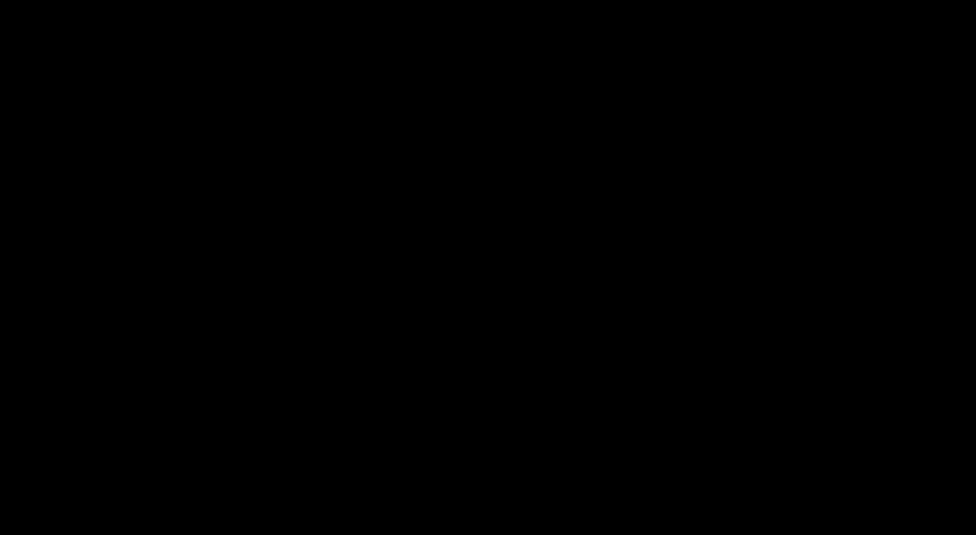
39. Micro-Measurements. High-Elongation Strain Measurements. *Tech Tip TT-605*, 4 (2015).

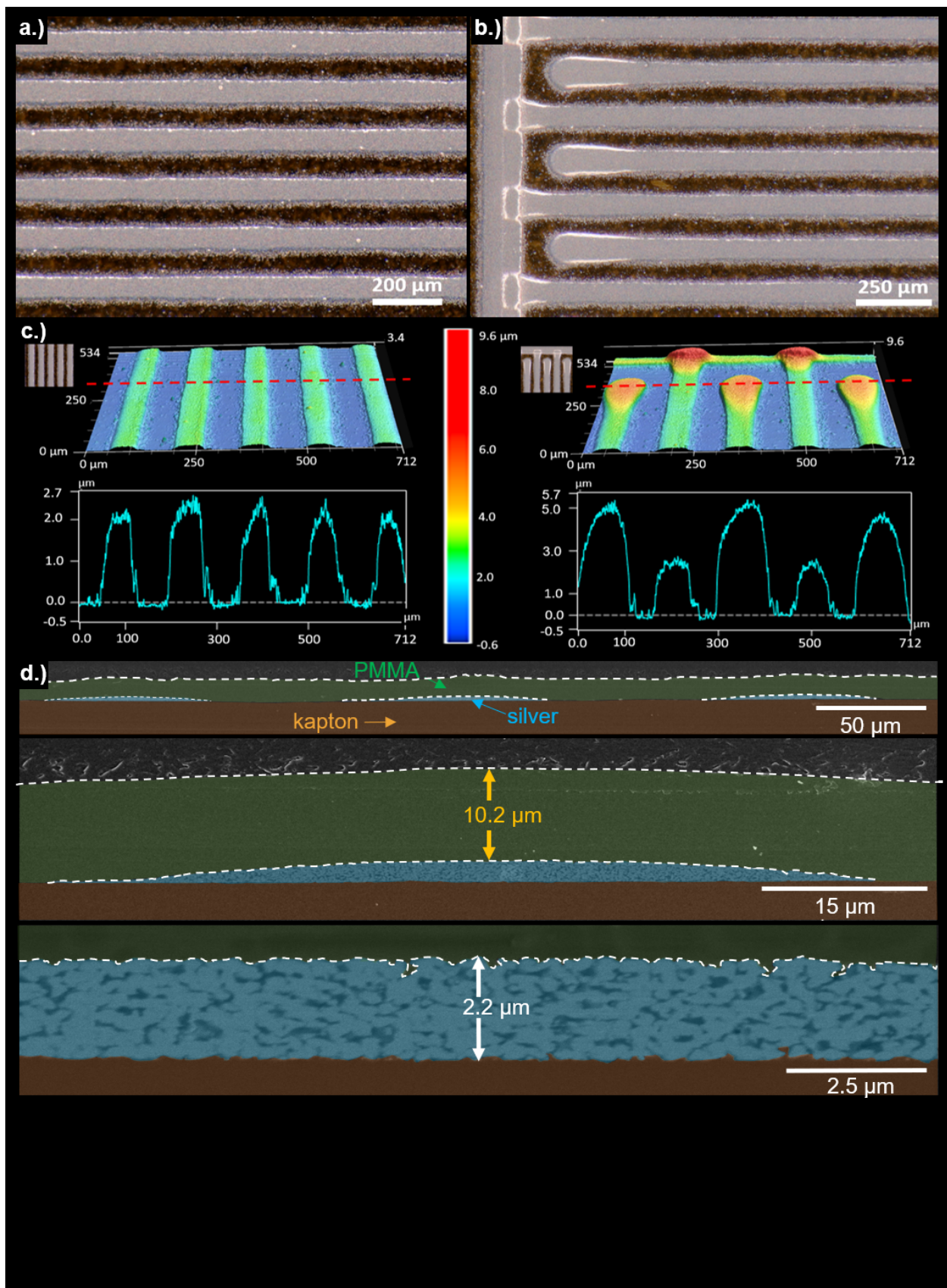
40. Tony R. Kuphaldt. Strain gauges. *Lessons Electr. Circuits, Vol. I – DC* 321–328 (2008).

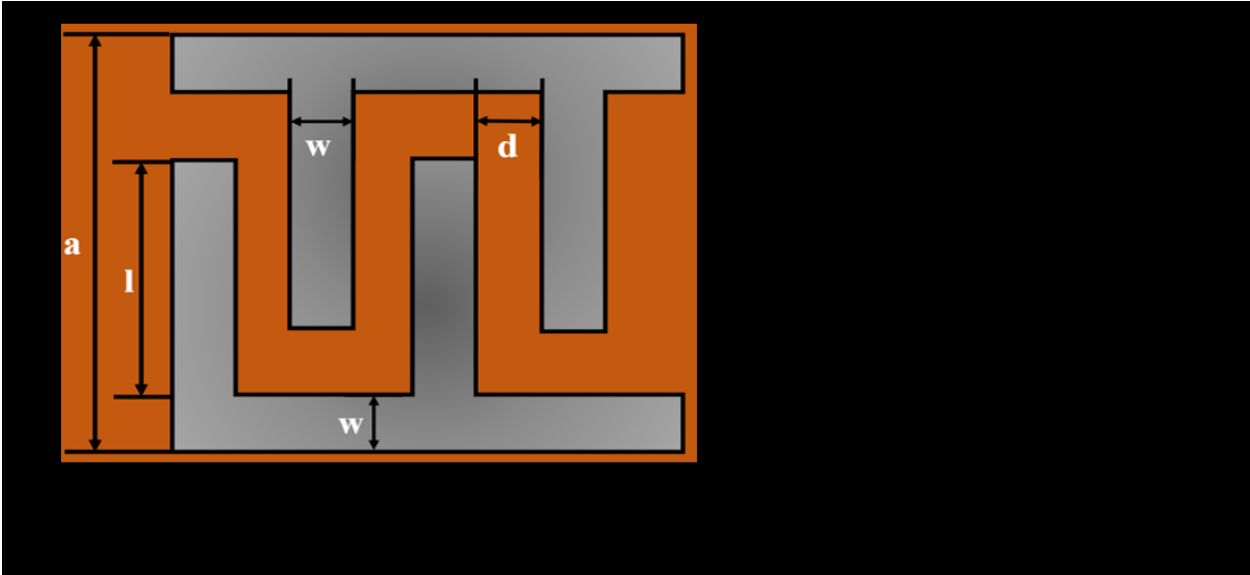
41. Manufacturing, A. R. Polychloroprene Rubber - neoprene datasheet.

*Polychloroprene Rubber - neoprene datasheet* (2020). Available at:

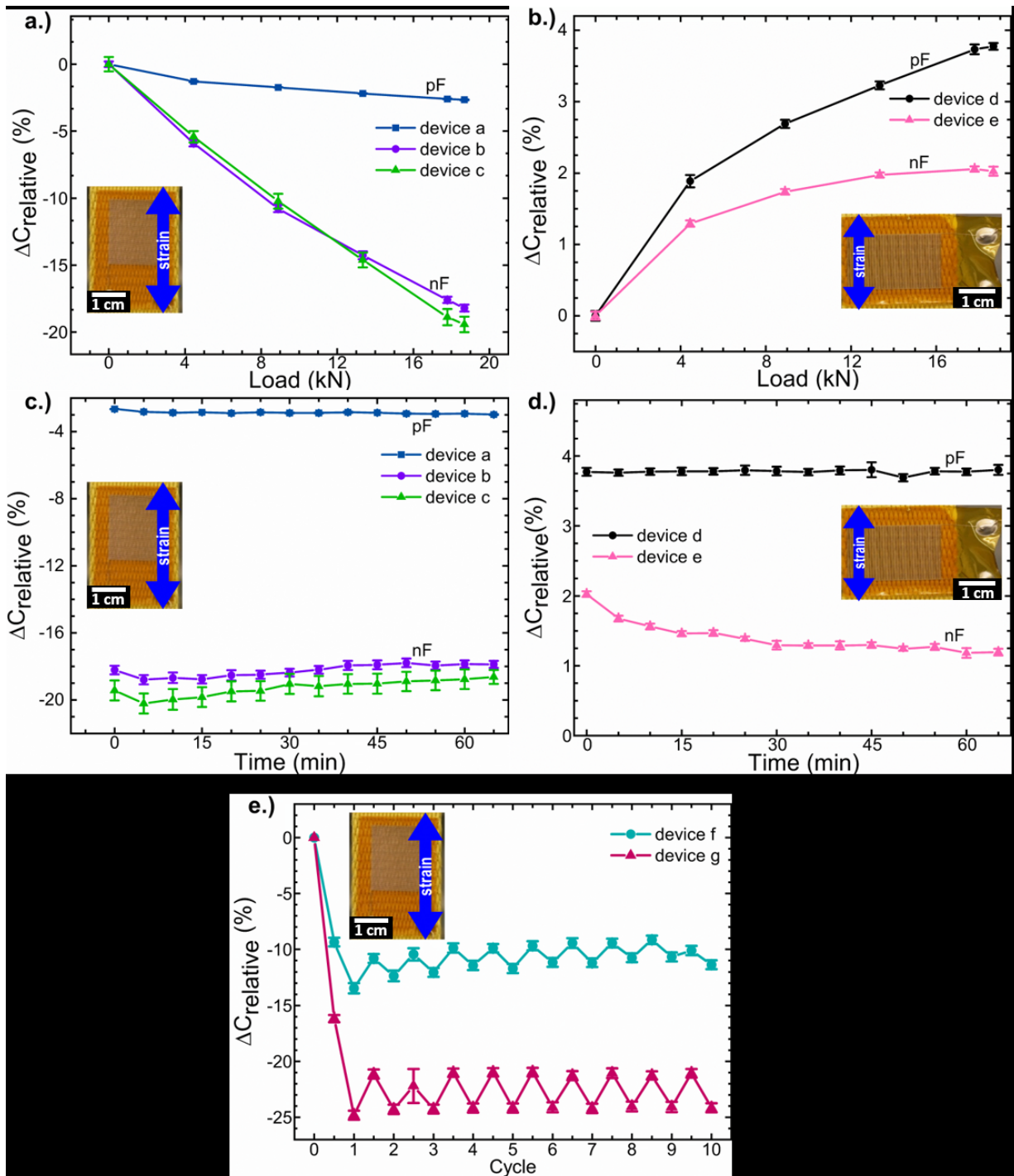
<http://www.amesrubberonline.com/pdf/polychloroprene-neoprene.pdf>. (Accessed: 15th April 2020)









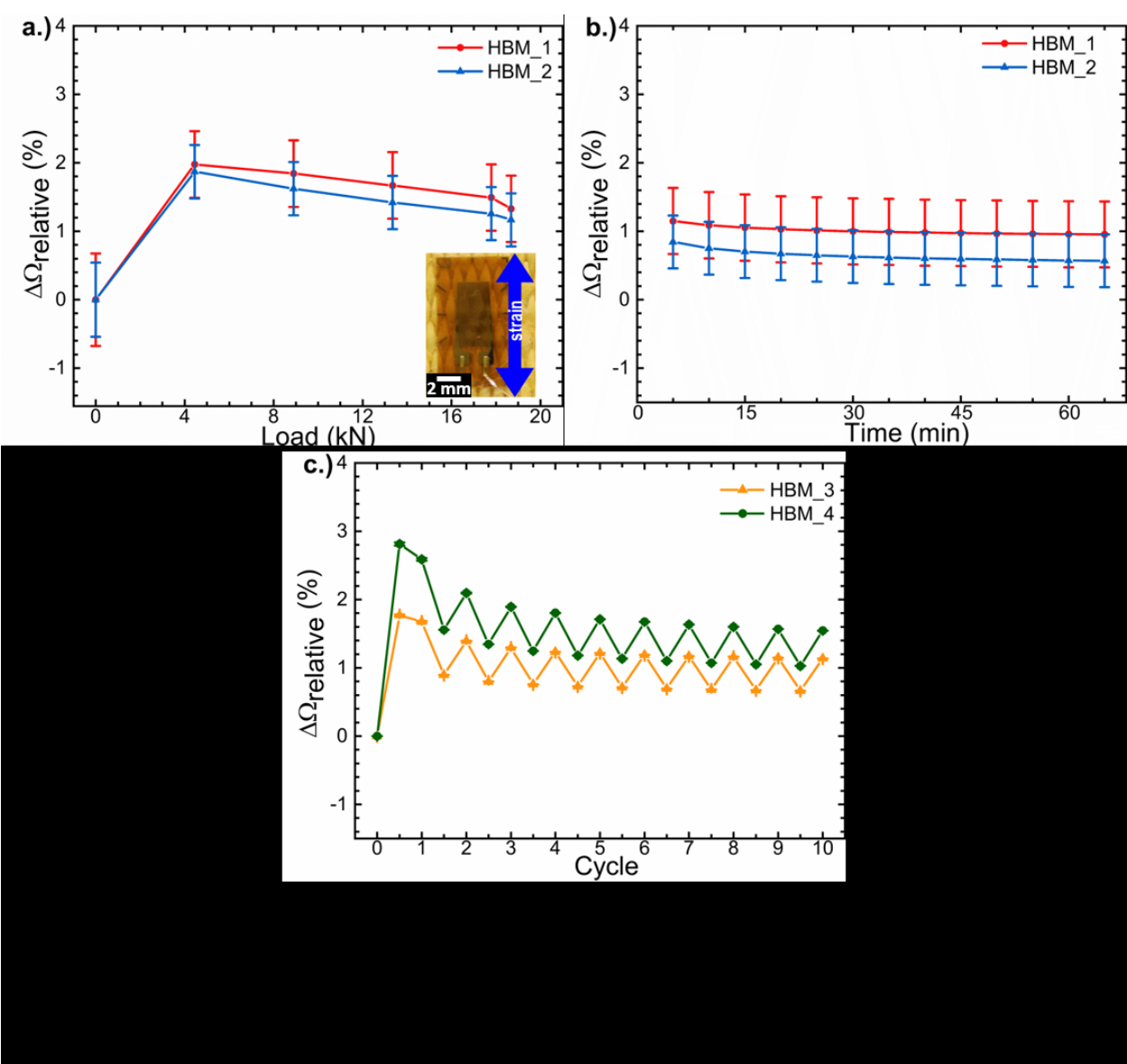


where a total of seven different devices were utilized for either dynamic (a-e), static (a-e), or cyclic (f-g) testing.

(devices a-c) (devices d-e) those same devices (devices a-c) (devices d-e) two different devices (f-g)

Bending test f.) for printed CSGs demonstrates a stable capacitance and good device flexibility for curvatures up to  $53 \text{ m}^{-1}$ .

626



627

628

629

630

631

632

633

634

635

